Patterned Nucleation Control in Vacuum Deposition of Organic Molecules

W. C. Wang,[1] D. Y. Zhong,[1] J. Zhu,[1] F. Kalischewski,[2] R. F. Dou,[1] K. Wedeking,[4] Y. Wang,[3] A. Heuer,[2] H. Fuchs,[1] G. Erker,[4] and L. F. Chi[1,*]

[1]*Physikalisches Institut and Center for Nanotechnology (CeNTech), Universität Münster, 48149 Münster, Germany*
[2]*Institut für Physikalische Chemie, Universität Münster, 48149 Münster, Germany*
[3]*Key Laboratory for Supramolecular Structure and Materials of the Ministry of Education, College of Chemistry, Jilin University, Changchun, 130012, China*
[4]*Organisch-Chemisches Institut, Universität Münster, 48149 Münster, Germany*

(Received 16 February 2007; published 1 June 2007)

We report a generally applicable method to pattern organic molecules on mesoscopic scales. In our method, organic molecular beam deposition was conducted on substrate surfaces prepatterned with materials to which the organic molecules have larger binding energies in comparison to the substrate. Fully uniform nucleation control at these predefined locations can be achieved by an appropriate selection of the growth parameters including temperature and deposition rate. The physical mechanisms involved are studied by Monte Carlo simulations and stand in good agreement with the experimental findings.

DOI: 10.1103/PhysRevLett.98.225504 PACS numbers: 61.66.Hq, 68.55.Ac, 81.15.−z, 85.40.Hp

Template-directed aggregation or crystallization is widely used to build architectures of functional materials [1–16]. In this technique, substrate surfaces are prepatterned to thermodynamically or kinetically modulate the aggregation of certain objects (atoms, molecules, and particles) at specific sites and/or orientations. Template-directed patterning in vacuum has been achieved for semiconducting quantum dots [1–6], nanofibers [7,8], and in solutions for inorganic crystals [9], nanoparticles [10], colloidal crystals [11], organic molecules [12], polymers [13], biological materials [14], and cells [15]. Very recently, patterned organic single crystals have been obtained from vapor deposition [16]. However, template-directed growth of organic assemblies by organic molecular beam deposition (OMBD) [17] yielding high uniformity is rarely reported.

In this Letter, we present a general method to pattern organic molecules by template-directed nucleation control on mesoscopic scales using OMBD under ultrahigh vacuum conditions. To control the nucleation process the substrate surface is prepatterned with materials on which the organic molecules have different binding energies from the substrate. Figure 1(a) schematically illustrates our concept for patterned growth of organic aggregates by nucleation control. The organic molecules are sublimated from a crucible and deposited on the substrate, where they diffuse along the surface. On an unpatterned substrate nuclei form when a critical number of molecules aggregates. This occurs stochastically and a random distribution of islands [Fig. 1(a), left] will be found. After saturation, they grow continuously due to the adsorption of further molecules. In contrast, on a prepatterned surface the molecules may prefer to nucleate on the prepatterned positions rather than the substrate due to a larger binding energy with the pattern material. The nucleation behavior is determined by the interplay of surface diffusion and deposition rate. In case surface diffusion cannot provide sufficient transport of the adsorbed molecules to the predefined positions, additional islands will nucleate between predefined positions. Under appropriate growth conditions (temperature and deposition rate), all nucleation will take place on the predefined positions [Fig. 1(a), right]. At this point, the mechanisms of our system differ essentially from the adsorption or desorption controlled mechanism recently reported in [16].

Experimentally we used silicon oxide [300 nm thick SiO_2 on Si(001)] as the substrate, which was patterned with gold dots by electron beam lithography followed by metal vapor deposition. We deposited diferrocene (diFc) [18], which is a derivative of ferrocene containing two

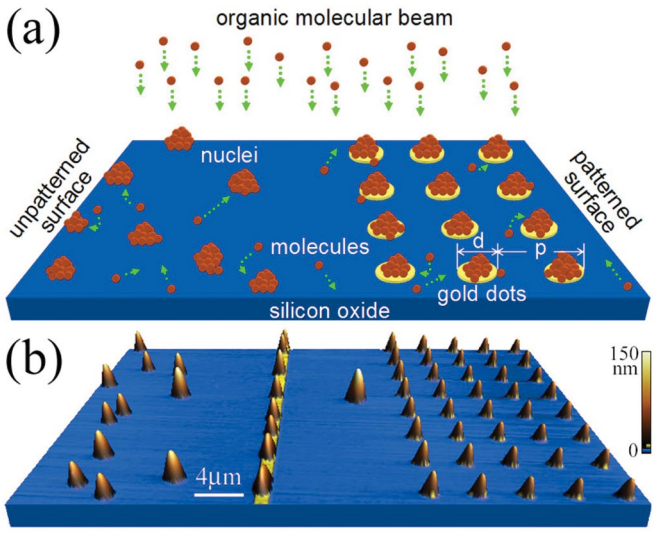

FIG. 1 (color online). Template-directed nucleation control for organic molecular deposition. (a) Schematic diagram. (b) AFM image of diFc patterned structure.

ferrocenyl groups bridged by an oligoethylene chain. The sample was grown at a temperature of 45 °C and a deposition rate of 0.1 nm/min with an average thickness of 2 nm. After deposition, organic islands were found as observed by atomic force microscopy (AFM). In the unpatterned region [left side of Fig. 1(b)] the islands were distributed randomly with an average height of 102.8 ± 17.6 nm. In the patterned region nucleation took place exclusively on the gold dots as shown in the right part of Fig. 1(b) (diameter $d = 1.0$ μm and periodicity $p = 4.0$ μm) with a more uniform height of 92.8 ± 5.2 nm. A 1.0 μm wide gold strip served as a separator between patterned and unpatterned regions [middle of Fig. 1(b)].

We further systematically studied the patterned growth of different organic substances with respect to the experimental parameters: namely, the template periodicity p, the diameter d of the gold dots, the growth temperature T, and the deposition rate F. The molecules and growth conditions were chosen to allow diffusion on a micrometer scale rather than nanometers as in [19].

For this study, we used N,N'-bis-(1-naphthyl)-N,N'-diphenyl-1,1′-biphenyl'-4,4′-diamine (NPB), which is a blue light emitting and classic hole transport material widely used in high performance organic light emitting diodes (OLEDs) [20]. NPB molecules formed randomly distributed islands when they were deposited on unpatterned SiO_2 at 133 °C, while they formed a continuous film on unpatterned Au substrate at the same temperature. Similar to diFc, uniform and regular arrays of NPB with p ranging from 450 nm up to 2.4 μm were successfully fabricated at a growth temperature of 133 °C and 138 °C. The height of the resulting organic islands, which mainly depends on p and d, has a narrow distribution with a standard deviation of typically less than 10% of the average height. The islands are domelike and the height as well as the size can be conveniently varied in a broad range by appropriate combinations of p, d, F, and deposition time.

One of the key issues concerning application is the realization of full nucleation control efficiency (NCE), which we define as $x_{NCE} = N_{Au}/N$ with N_{Au} and N representing the number of gold dots and the total number of islands, respectively. The experimentally accessible parameters governing x_{NCE} at a given p are the growth temperature and the deposition rate. For example, at the same p and F, full NCE was obtained for NPB at a temperature of 138 °C but not at 133 °C. Varying the deposition rate at constant p and T, $x_{NCE} = 1$ was obtained for NPB molecules deposited with $F = 0.1$ nm/min, while additional nuclei appeared between the gold dots at an increased rate of 0.3 nm/min.

To compare different systems we introduce the characteristic length scale λ, which we derive from the island density (N/A) (where A is the area) of an unpatterned substrate as $\lambda = (N/A)^{-1/2}$. This way, λ is a measure for the distance between adjacent islands. Using λ, we introduce the dimensionless periodicity $p^* = p/\lambda$, which enables us to directly compare x_{NCE} of different experiments in the same graph (Fig. 2). For example, diFc grown on silicon oxide at 45 °C yielded $\lambda = 5.8$ μm. The experimental NCE of this system grown on gold dot arrays with $d = 1.5$ μm and p between 2.0 and 12.0 μm is shown as red diamonds in Fig. 2. As expected, at small p^* we achieved nearly complete NCE, until at a critical value around $p^* = 1$ new islands form and x_{NCE} begins to decrease. Similar results were obtained for experiments with NPB at 123 °C (violet stars), 133 °C (green triangles), and 138 °C (black squares), with λ equal to 1.7, 2.3, and 2.5 μm, respectively. The similar behavior of different materials at different temperatures indicates that template controlled nucleation is governed by a general mechanism.

To gain deeper insight into this mechanism, computer simulations were conducted. The silicon oxide substrate (S), the gold dot (A), and the deposited molecules (M) were taken into account as individual particles. The substrate was constructed out of a fcc lattice exhibiting a (111) surface with dimensions of $(na) \times (\sqrt{3}na/2)$ with a as the nearest-neighbor distance in the S crystal and n representing the number of "unit cells" in the x dimension. Thus, a nearly quadratic shape of the substrate area was obtained. Periodic boundary conditions were applied, generating a quasi-infinite surface. A three-layer A dot with a diameter of $6a$ was located at the center of the surface. Different p was realized by variation of n. To enhance simulation efficiency, A and S particles were considered

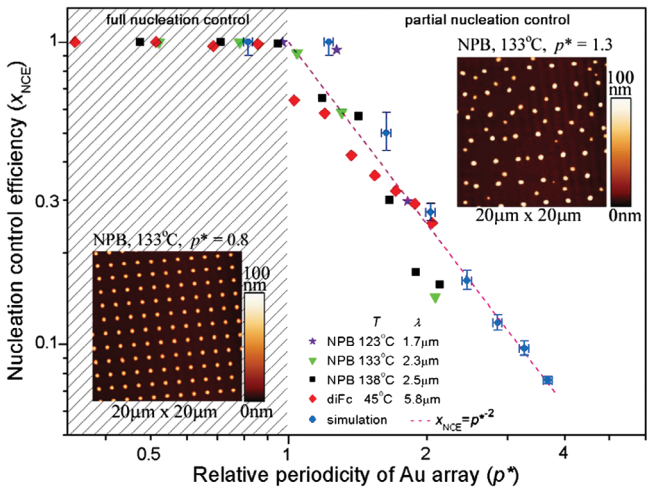

FIG. 2 (color online). Relationship between the nucleation control efficiency (x_{NCE}) and the relative periodicity (p^*) obtained from experiments and MC simulations. When $p^* < 1$, x_{NCE} nearly equals unity, indicating the full control of nucleation. When $p^* > 1$, x_{NCE} is gradually decreased, indicating partial control of nucleation. The dashed pink line shows the relationship $x_{NCE} = p^{*-2}$, which should hold for $x_{NCE} \ll 1$. Insets are AFM images of NPB grown at 133 °C, showing full nucleation control at $p^* = 0.8$ (left) and partial nucleation control at $p^* = 1.3$ (right).

static during the simulation. Since the molecules are much smaller than the length scales of the experiment, we used simple Lennard-Jones (LJ) pair potentials to mimic the molecular interactions. The interaction parameters of the LJ potential were chosen as $\varepsilon_{MA}/k_BT = 5$, $\varepsilon_{MM}/k_BT = 3.7$, and $\varepsilon_{MS}/k_BT = 1.5$, and the radial constants $\sigma_{i,j}$ as $2^{-1/6}a$. The cutoff is $2.5\sigma_{i,j}$. Propagation was achieved by means of an off-lattice Monte Carlo (MC) algorithm common to nucleation and crystallization problems [21]. Typically, approximately 1.5 molecules per substrate-surface atom were deposited during one simulation run of approximately $1–5 \times 10^6$ steps until a constant number of islands was reached. If an M particle moved to a position of larger distance than the cutoff from the closest particle, it was considered desorbed and removed from the simulation. For each size of the system six independent simulations were conducted to obtain an averaged number of islands.

After a sufficiently long simulation time the number of islands saturates and a quasiequilibrium distribution can be obtained. The value of λ was determined in a separate simulation without A dots. Then, p^* and x_{NCE} were calculated in analogy to the experimental procedure and are depicted as circles in Fig. 2. The simulation results are well consistent with the experimental outcome, as for $p^* < 1$ all aggregation occurs on the dots and in the vicinity of p^* additional nuclei start to appear. Thus, the physical mechanism of island formation is indeed very general and independent of microscopic details.

Supposing that in the regime of large periodicity (with $p \gg \lambda$ and $x_{NCE} \ll 1$) the influence of the gold dots on the island density is very small, we obtain the same nucleus density as on the unpatterned surface. This $x_{NCE} = p^{*-2}$ behavior is represented by the dashed pink line of Fig. 2 and stands in good agreement with the experimental and numerical data. Furthermore, nucleation theory [22] tells that $(N/A) \propto (F/D)^{\chi}$, with $1/3 < \chi < 1$ depending on the critical nucleus size. Thus, λ decreases with increasing deposition rate and decreasing diffusion coefficient (e.g., via decreasing T), both in qualitative agreement with our experimental observations. In this way, one can estimate the effect of external parameters like growth temperature on the NCE. Furthermore, for x_{NCE} approaching unity the cubic symmetry of the gold dots becomes relevant and deviations from $x_{NCE} = p^{*-2}$ may occur, rendering the dependence of x_{NCE} on p^* nonuniversal.

As described above, both experimental and simulation results indicate that full nucleation control can be obtained, if the periodicity of the pattern is similar to or smaller than the characteristic length scale. Based on this rule, we have succeeded in fabricating organic patterns with different features. Figure 3(a) illustrates a concentric ring pattern consisting of Au lines with different widths but separated by equal distances. The height of the deposited NPB layer on the Au lines is well adjustable by the prepatterns. In

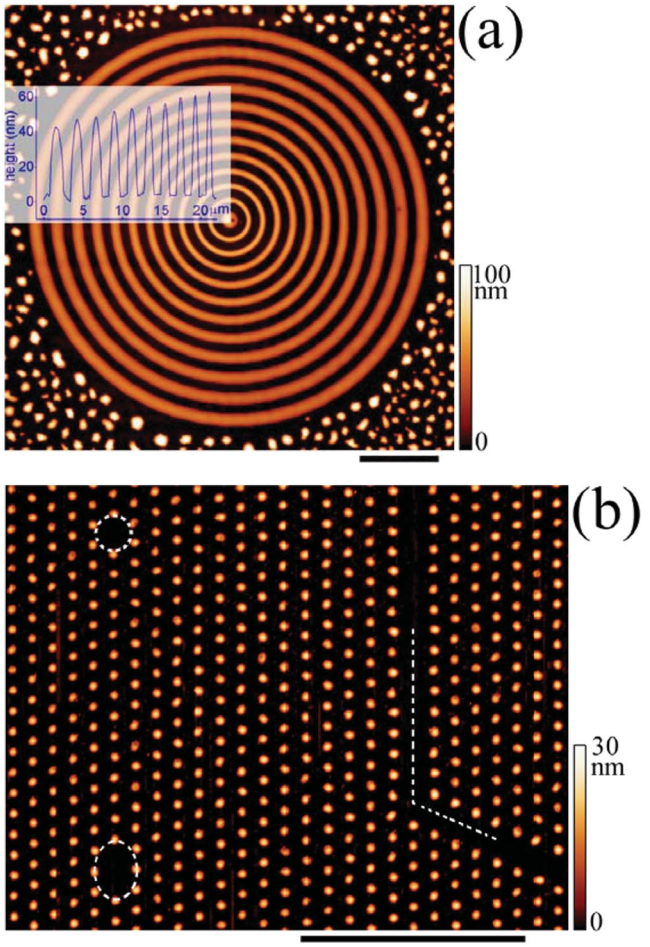

FIG. 3 (color online). Organic patterns with concentric rings and artificial defects. Scale bars, 10 μm. (a) AFM of an NPB concentric ring pattern with ring width from 600 nm (inside) to 1.7 μm (outside) and spacing between the rings of 800 nm. Inset: Height profile showing the modulation of the occupation ratio to the organic layer thickness. (b) AFM of artificial defects in an NPB hexagonal dots array with a dot diameter of 300 nm and periodicity of 900 nm. The single-point, double-point, and line vacancies are marked by a circle, an ellipse, and a line, respectively.

Fig. 3(b), a pattern with defect structure is presented. In addition to diFc and NPB, we have also successfully fabricated patterns of several other organic molecules, indicating the flexibility and the controllability of this method.

The above approach provides a versatile means to fabricate large-area uniform organic structures with high resolution, meeting the demands for, e.g., microdisplays at micrometer scale or two-dimensional photonic structures for light emissive organic molecules. The latter provide the possibility to increase the extraction efficiency of OLEDs in a way analogous to inorganic semiconducting diodes [23]. By combination with parallel processes such as nanoimprinting, the prepatterned structure can be designed and fabricated with submicrometer to sub-100 nm resolution

and high output. Since the production of organic structures is completely carried out under vacuum, this method has the advantage to avoid ambient contamination (water and oxygen) and is readily compatible with matured semiconductor processing technology.

The authors thank M. Hirtz (Universität Münster, Germany) for data analysis and NanoAnalytics GmbH for help on pattern fabrication.

*Corresponding author.
Email address: chi@uni-muenster.de

[1] Z. Zhong and G. Bauer, Appl. Phys. Lett. **84**, 1922 (2004).
[2] G. Chen, H. Lichtenberger, G. Bauer, W. Jantsch, and F. Schäffler, Phys. Rev. B **74**, 035302 (2006).
[3] G. Jin, J. L. Liu, and K. L. Wang, Appl. Phys. Lett. **76**, 3591 (2000).
[4] G. S. Kar, S. Kiravittaya, M. Stoffel, and O. G. Schmidt, Phys. Rev. Lett. **93**, 246103 (2004).
[5] J. T. Robinson *et al.*, Nano Lett. **5**, 2070 (2005).
[6] T. Kitajima, B. Liu, and S. R. Leone, Appl. Phys. Lett. **80**, 497 (2002).
[7] H. J. Fan, P. Werner, and M. Zacharias, Small **2**, 700 (2006).
[8] Z. F. Ren *et al.*, Appl. Phys. Lett. **75**, 1086 (1999).
[9] J. Aizenberg, A. J. Black, and G. M. Whitesides, Nature (London) **398**, 495 (1999).
[10] N. Lu *et al.*, Nano Lett. **4**, 885 (2004).
[11] A. van Vlaaderen, R. Ruel, and P. Wiltzius, Nature (London) **385**, 321 (1997).
[12] A. L. Briseno *et al.*, J. Am. Chem. Soc. **127**, 12 164 (2005).
[13] B. Dong, D. Y. Zhong, L. F. Chi, and H. Fuchs, Adv. Mater. **17**, 2736 (2005).
[14] A. S. Blawas and W. M. Reichert, Biomaterials **19**, 595 (1998).
[15] M. Veiseh and M. Zhang, J. Am. Chem. Soc. **128**, 1197 (2006).
[16] A. L. Briseno *et al.*, Nature (London) **444**, 913 (2006).
[17] S. R. Forrest, Chem. Rev. **97**, 1793 (1997).
[18] K. Wedeking *et al.*, Chem. Eur. J. **12**, 1618 (2006).
[19] J. V. Barth, G. Costantini, and K. Kern, Nature (London) **437**, 671 (2005).
[20] S. A. Van Slyke, C. H. Chen, and C. W. Tang, Appl. Phys. Lett. **69**, 2160 (1996).
[21] A. C. Levi and M. Kotrla, J. Phys. Condens. Matter **9**, 299 (1997).
[22] T. Michely and J. Krug, *Islands, Mounds, and Atoms: Patterns and Processes in Crystal Growth Far from Equilibrium* (Springer-Verlag, Berlin, 2003).
[23] S. Fan, P. R. Villeneuve, J. D. Joannopoulos, and E. F. Schubert, Phys. Rev. Lett. **78**, 3294 (1997).